
RFWAVE: MULTI-BAND RECTIFIED FLOW FOR AUDIO WAVEFORM RECONSTRUCTION

Peng Liu
laupeng1989@gmail.com

Dongyang Dai
accum.dai@gmail.com

ABSTRACT

Recent advancements in generative modeling have led to significant progress in audio waveform reconstruction from diverse representations. Although diffusion models have been used for reconstructing audio waveforms, they tend to exhibit latency issues because they operate at the level of individual sample points and require a relatively large number of sampling steps. In this study, we introduce RFWave, a novel multi-band Rectified Flow approach that reconstructs high-fidelity audio waveforms from Mel-spectrograms. RFWave is distinctive for generating complex spectrograms and operating at the frame level, processing all subbands concurrently to enhance efficiency. Thanks to Rectified Flow, which aims for a flat transport trajectory, RFWave requires only 10 sampling steps. Empirical evaluations demonstrate that RFWave achieves exceptional reconstruction quality and superior computational efficiency, capable of generating audio at a speed 90 times faster than real-time¹.

1 Introduction

The advent of neural network-based generative models has revolutionized the generation and synthesis of audio, showcasing remarkable advancements in artificial intelligence. These models are adept at learning the nuances of training data distributions, enabling them to reconstruct new, similar data points. In particular, waveform reconstruction has emerged as a key application of these generative models.

A key focus in speech technology research is on reconstructing high-quality waveforms from compact representations, such as Mel-spectrograms or phoneme sequences. WaveNet [1], a convolution-based autoregressive model, marked a major breakthrough in this domain through the use of neural network-based generative models for waveform reconstruction. The quality of waveforms produced by WaveNet significantly exceeds that of previous signal processing methods like WORLD [2]. However, the sequential, sample-by-sample waveform reconstruction approach of WaveNet leads to substantial computational demands. To more effectively harness the capabilities of recurrent networks, WaveRNN [3] was developed, employing an RNN in an autoregressive model for waveform reconstruction, optimizing the use of recurrent network characteristics.

The inherent slowness of autoregressive models, which predict samples one after another, has prompted interest in parallel waveform reconstruction. This has led to the development of models like Parallel WaveNet [4] and ClariNet [5]. Concurrently, the emergence of Generative Adversarial Networks (GANs) [6] has given rise to parallel GAN-based waveform reconstruction methods, such as Mel-GAN [7], ParallelWaveGAN [8], and HiFi-GAN [9]. These approaches generally offer faster reconstruction speeds, attributing to their generators' simpler model structures compared to prior parallel methods.

Considering that speech signals consist of a high number of samples per second, modeling speech waveforms typically involves intricate neural networks, which incorporate upsampling layers. The incorporation of ISTFT in replacing some upsampling layers of the model, shifting its task to predicting the complex spectrograms rather than directly reconstructing the waveform, effectively refines the model structure and enhances computational efficiency. Models such as iSTFTNET [10], Vocos [11], and APNet2 [12], which are grounded in GAN frameworks, have effectively used

¹Code is available at <https://github.com/bfs18/rfwave>

this method in reconstructing waveforms. They have achieved faster processing speeds and increased efficiency, all while maintaining the quality of the speech.

Nevertheless, GAN-based waveform reconstruction models [7, 8, 9, 10, 11] often require intricate discriminator designs for high-quality output and may face issues like instability and mode collapse. To address these challenges, researchers have investigated diffusion models for reconstructing waveforms, as seen in studies like Diffwave [13], WaveGrad [14], and Multi-Band Diffusion [15]. However, diffusion-based models typically necessitate multiple sampling steps for synthesizing high-quality audio, leading to significant computational costs.

In this paper, we introduce a novel waveform reconstruction model based on Rectified Flow [16], which ensures high-quality output while also significantly enhancing overall efficiency. Our main contributions are summarized as follows:

1. By adopting the Rectified Flow and a innovative time-balanced loss, our model can reconstruct high-quality waveforms with a drastically reduced number of sampling steps.
2. We implement a multi-band approach that generates different sub-bands in parallel, ensuring audio quality while avoiding cumulative errors and enhancing synthesis speed.
3. Our model operates at the level of STFT frames, not individual waveform sample points. This approach significantly enhances processing speed.

Our experimental results confirm that our model is capable of generating high-fidelity audio waveforms and performing inference at speeds up to 90 times faster than real-time.

2 Background

Rectified Flow Rectified Flow [16] presents an innovative ODE-based framework for generative modeling and domain transfer. It introduces a method to learn a transport mapping that connects two distributions, π_0 and π_1 on \mathbb{R}^d , based on empirical observations:

$$\frac{dZ_t}{dt} = v(Z_t, t), \quad \text{initialized from } Z_0 \sim \pi_0, \text{ such that } Z_1 \sim \pi_1, \quad (1)$$

where $v: \mathbb{R}^d \times [0, 1] \rightarrow \mathbb{R}^d$ represents a velocity field. The learning of this field involves minimizing a mean square objective function,

$$\min_v \mathbb{E}_{(X_0, X_1) \sim \gamma} \left[\int_0^1 \left\| \frac{d}{dt} X_t - v(X_t, t) \right\|^2 dt \right], \quad \text{with } X_t = \phi(X_0, X_1, t), \quad (2)$$

where $X_t = \phi(X_0, X_1, t)$ represents a time-differentiable interpolation between X_0 and X_1 , with $\frac{d}{dt} X_t = \partial_t \phi(X_0, X_1, t)$. The γ represents any coupling of (π_0, π_1) . An illustrative instance of γ is the independent coupling $\gamma = \pi_0 \times \pi_1$, which allows for empirical sampling based on separately observed data from π_0 and π_1 . The authors recommended a simple choice of

$$X_t = (1 - t)X_0 + tX_1 \implies \frac{d}{dt} X_t = X_1 - X_0. \quad (3)$$

This simplification results in linear trajectories, which are critical for accelerating the inference process. Typically, the velocity field v is represented using a deep neural network. The solution to (2) is approximated through stochastic gradient methods. To approximate the ODE presented in (1), numerical solvers are commonly employed. A prevalent technique is the forward Euler method. This approach computes values using the formula

$$Z_{t+\frac{1}{n}} = Z_t + \frac{1}{n} v(Z_t, t), \quad \forall t \in \{0, \dots, n-1\}/n, \quad (4)$$

where the simulation is executed with a step size of $\epsilon = 1/n$ over n steps.

The velocity field has the capacity to incorporate conditional information. This is particularly essential in applications like text-to-image generation, where a text prompt is a critical factor. Consequently, in such contexts, $v(Z_t, t)$ in (2) is modified to $v(Z_t, t | \mathcal{C})$, where \mathcal{C} represents the conditional information pertinent to the corresponding X_1 .

Estimating Complex Spectrograms Waveform reconstruction from complex spectrograms can be effectively achieved using the Inverse Short-Time Fourier Transform (ISTFT). Notably, Vocos [11] and APNet2 [12], utilizing GANs as their model framework, estimate magnitude and phase spectrograms from the input Mel spectrograms,

which can be transformed to complex spectrograms effortlessly. Both models operate at the frame level, enabling them to achieve significantly faster inference speeds compared to HiFi-GAN [9], which uses multiple upsampling layers and operates at the level of waveform sample points. Moreover, these models preserve the quality of the synthesized waveform, demonstrating their superiority in both speed and fidelity without a trade-off. In this paper, we directly estimate complex spectrograms using Rectified Flow and focus on frame-level operations, aiming to enhance both the efficiency and quality of our waveform synthesis process.

Multi-band Audio Waveform Reconstruction Both Multi-band MelGAN [17] and Multi-band Diffusion [15] employ multi-band strategies, albeit for different purposes within their respective frameworks. Multi-band MelGAN, specifically, uses Pseudo-Quadrature Mirror Filters (PQMF) [18] to divide frequency bands. This division results in each subband’s waveform being a fraction of the original waveform’s length, based on the number of subbands. By reshaping these subbands into feature dimensions and utilizing a unified backbone for modeling, Multi-band Melgan is able to operate on considerably shorter signals. This strategy significantly enhances the efficiency of the model, leading to accelerated training and inference processes. Multi-band Diffusion utilizes an array of band-pass filters to separate the frequency bands and models each subband with a distinct model. This approach ensures that errors in one band do not negatively impact the others. In our research, we simplify the process of frequency band division by directly choosing the appropriate dimensions from the complex spectrograms. Furthermore, we enhance efficiency by modeling all subbands together in parallel with a single, unified model. This strategy improves the processing speed and also helps in reducing error accumulation across different subbands.

3 Method

Our model utilizes a multi-band Rectified Flow to directly predict the complex spectrogram. It operates at the STFT frame level and incorporates a highly efficient ConvNeXtV2 [19] backbone. With only 10 steps of sampling, the model is capable of producing high-quality waveforms.

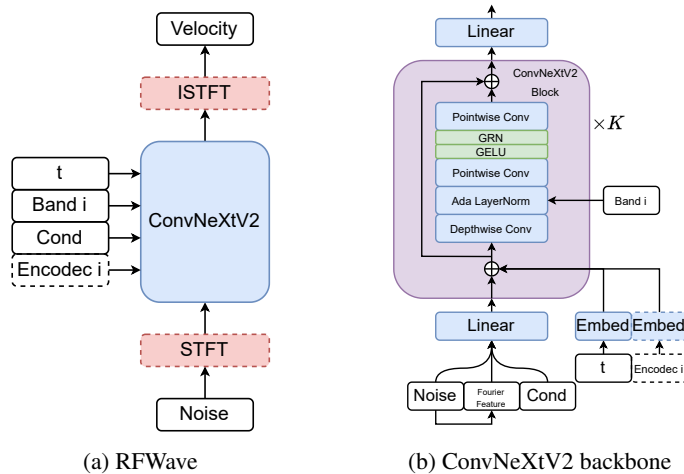


Figure 1: The overall structure for RFWave. $\text{Band } i$ is the subband index, Cond is the conditional input, and $\text{Encodec } i$ is the Encodec bandwidth index. The blue boxes represent modules that contain trainable parameters, while the green boxes symbolize modules without trainable parameters. Modules enclosed in a dashed box are considered optional.

3.1 Multi-band Rectified Flow

In our initial experiments, we observe that attempts to predict the full-band complex spectrogram result in a compromised quality of waveform reconstruction. To address this, we shift our approach to a multi-band structure. It introduces error accumulation when conditioning higher bands on lower bands, whereby inaccuracies in the lower bands adversely affects the higher bands during the inference stage, as noted in [15]. Consequently, we design our model by not employing the lower band as a conditional input for the higher band. This structure yields an additional benefit: the ability to predict all frequency bands concurrently, thereby significantly diminishing the inference latency. We can batch the different bands of a sample to facilitate simultaneous training or inference.

The model structure is depicted in Figure 1a. All frequency bands share the model, distinguished by a unique subband index. For each subband, the corresponding noise is fed into the ConvNeXtV2 backbone to predict the velocity conditioned on time t , the subband index, conditional input (the Mel spectrogram or the Encodec [20] embedding), and an optional Encodec bandwidth index. The detailed structure of the ConvNeXtV2 backbone is shown in Figure 1b. We employ Fourier features as described in [21]. The noise, Fourier features, and conditional inputs are concatenated and then passed through a linear layer, forming the input that is fed into a series of ConvNeXtV2 blocks. The sinusoidal time embedding, along with the optional Encodec bandwidth index embedding, are element-wise added to the input of each ConvNeXtV2 block. Furthermore, the subband index is incorporated via an adaptive layer normalization module, which utilizes learnable embeddings as described in [22, 11]. The other components are identical to those within the ConvNeXtV2 architecture, details can be found in the [19].

3.2 Operating in Time Domain or Frequency Domain

Our model is designed to function at the STFT frame level, with the flexibility to operate in either the time or frequency domain. In the time domain, as shown in Figure 1a, the signal and noise are both inherently temporal, necessitating the use of STFT and ISTFT. Conversely, in the frequency domain, both noise and velocity are represented in this domain, eliminating the need for STFT and ISTFT. For the time domain, noise and velocity adhere to dimensions of $[1, T]$, where T represents the waveform length in sample points². Notably, only subband i is processed after STFT and prior to ISTFT in a single feed-through, in line with our prior discussion. In the frequency domain, the dimensions of noise and velocity shift to $[d_s, F]$, with d_s denoting the dimension of a subband’s complex spectrum and F the number of frames. Here, the real and imaginary parts are concatenated to form a d -dimensional complex spectrum feature. During the inference stage, the model operating in the time domain includes two additional operations—STFT and ISTFT—at each step compared to the model operating in the frequency domain. Despite this, it demonstrates slightly superior performance, particularly in capturing high-frequency details. The details of the comparative experiments are provided in Section 5.

3.3 Waveform Equalization or STFT Normalization

A white Gaussian noise signal has uniform energy distribution across all frequency bands. However, the energy profiles of various waveform types vary markedly among different frequency bands. For instance, the energy in a speech waveform exhibits an exponential decay with increasing frequency, whereas a music waveform tends to maintain a more consistent energy distribution across frequencies. These disparities pose challenges for training diffusion models. Consequently, it becomes advantageous to equalize the energy across waveform frequency bands [15].

In the time-domain model, a bank of Pseudo-Quadrature Mirror Filters (PQMF) is employed to decompose the input waveform into subbands. Subsequently, these subbands are equalized and then recombined to form the equalized waveform. The performance of the PQMF bank exhibits a modest enhancement compared to the array of band-pass filters employed in [15]. In the frequency-domain model, the waveform is transformed a complex spectrogram without equalization. Subsequent processing involves the dimension-wise normalization of the complex spectrogram feature. Mean-variance normalization, utilizing the running averages of mean and variance computed during training, is applied for both waveform equalization and STFT normalization. This approach ensures that the transformation can be effectively inverted using the same running average statistics.

3.4 Time-balanced Loss

In our preliminary experiments, we observe the presence of low-volume noise in regions that are expected to be silent. We attribute this to the property of mean square error (MSE) used in (2). The MSE measures the absolute distortion between the predicted values and the ground truth. Since the values in silent regions are close to zero, even a minor absolute distortion in predictions can lead to a significant relative error. Consequently, models trained with the MSE produce small absolute distortions in silent regions, which are then perceived as noise.

We propose a time-balanced loss to mitigate this problem. Our time-balanced loss is designed to weight errors differently depending on the region’s volume across the time-axis. Specifically, for each frequency subband, we compute the standard deviation along the feature dimension of the ground truth velocity to construct a weighting coefficient of size $[1, F]$. This vector is reflective of the temporal volume of the respective subband, as depicted in Figure A.1. Subsequently, both the ground truth and predicted velocity are divided by this vector before proceeding to

²For simplicity, the batch dimension is not included in the discussion.

the subsequent steps. For the frequency domain model, the training objective defined in (2) is adjusted as follows:

$$\min_v \mathbb{E}_{X_0 \sim \pi_0, (X_1, C) \sim D} \left[\int_0^1 \| (X_1 - X_0)/\sigma - v(X_t, t | C)/\sigma \|^2 dt \right], \quad (5)$$

with $\sigma = \sqrt{\text{Var}_1(X_1 - X_0)}$ and $X_t = tX_1 + (1 - t)X_0$,

where D represents the dataset with paired X_1 and C , and Var_1 calculates the variance along the feature dimension. For the time domain model, this time balancing operation precedes the ISTFT process. This approach helps to minimize the relative error in low-volume regions. Our experimental results demonstrate that this method enhances overall performance, benefiting not just the silent parts. In an alternative interpretation, the equalization or normalization discussed previously brings the features closer to a standard normal distribution along the feature dimension. Simultaneously, the time-balanced loss aligns the features more closely with a standard normal distribution along the temporal dimension, prior to the calculation of the original MSE. This approach provides a more nuanced adjustment of the features, facilitate the training of Rectified Flow.

4 Experiments

Overview Initially, we evaluate models operating in both the time and frequency domains on the LJSpeech [23] dataset, assessing their performance variations with and without the incorporation of time-balanced loss. Following this preliminary assessment, the configuration yielding the best results undergoes further evaluation in diverse auditory scenarios, including singing, music, and extensive speech datasets, to determine its comprehensive applicability and efficiency.

Data For the singing data, we utilize the Opencpop dataset [24], comprising 100 high-quality Mandarin songs performed by a professional female singer. Regarding the music data, we employ the MTG-Jamendo dataset [25], featuring over 55,000 full-length audio tracks, annotated with 195 tags spanning genres, instruments, and mood/theme categories. For a comprehensive collection of speech data, we resort to the LibriTTS corpus, a multi-speaker English dataset encompassing roughly 600 hours of recordings made in diverse environments. Additionally, for speech data, we expand our training to a broader dataset encompassing LibriTTS-R[26], Aishell-3[27], VCTK[28], and the HQ-TTS mentioned in [29]. To ensure audio quality, we evaluate each speaker’s recordings within this dataset using the WADA[30] tool, excluding speakers whose majority of tracks exhibit a Signal-to-Noise Ratio (SNR) below 25dB. We refer to this dataset as Universal in the following discussion. For LJSpeech, we allocate 250 sentences for testing. We set apart 20 segments for the Opencpop test. The test-clean is employed for LibriTTS. The LibriTTS-R test-clean is used for Universal. Lastly, we reserve 1397 audio files for the Jamendo test.

We preserve the original sampling rates: LJSpeech at 22.05 kHz, LibriTTS and Universal at 24 kHz, and compute the Mel-scaled spectrograms with $n_fft = 1024$, $hop_length = 256$, and the number of Mel bins set to 100. For Opencpop and MTG-Jamendo, we keep the original 44.1 kHz sampling rate and compute the Mel-scaled spectrograms with $n_fft = 2048$, $hop_length = 512$, and again set the number of Mel bins to 100. When extracting the complex coefficients utilized by the model, we use the orthonormal Fast Fourier Transform (FFT) and its inverse (IFFT), with the normalization convention of dividing by $1/\sqrt{N}$ for both operations, here N is the number of FFT points. This approach ensures the spectrogram extracted is within a more reasonable range for modeling.

Implementation The RFWave backbone contains 8 ConvNeXtV2 blocks. Within each ConvNeXtV2 block, the depth-wise convolutional layer featuring a large kernel utilizes a kernel size of 7 and maintains a channel dimension of 512. The first and last 1×1 point-wise convolutional layers in the sequence possess channel dimensions of 512 and 1536, respectively. As described in Subsection 3.1, the complex spectrogram is divided into 8 equally spanned subbands. Those subbands are not related to the waveform equalization subbands mentioned in Subsection 3.3.

During training, audio samples are randomly cropped to lengths of 32512 and 65024 for 22.05/24 kHz and 44.1 kHz waveforms, respectively. This is equivalent to a crop window of 128 frames for both sampling rates. We use a batch size of 64. The model optimization is performed using the AdamW optimizer with a starting learning rate of $2e-4$ and beta parameters of (0.9, 0.999). A cosine annealing schedule is applied to reduce the learning rate to a minimum of $2e-6$. For evaluation purposes, we use 10 sampling steps unless otherwise stated.

Baseline and Evaluation Metrics We benchmark our RFWave model against Vocos [11]. We adopt the original training details to retrain Vocos for the LJSpeech and Opencpop datasets. For the LibriTTS dataset, we utilize the pre-trained model. To assess our models, we employ the UTMOS [31] for automatic prediction of Mean Opinion Scores (MOS), which acts as a proxy for subjective human assessments. We incorporate additional metrics into our

evaluation framework as well. These metrics include the Perceptual Evaluation of Speech Quality (PESQ) and Mel Spectral Signal-to-Noise Ratio (Mel-SNR) as proposed in [15]. Mel-SNR measures the fidelity of the mel-spectrogram of the reconstructed signal compared with the ground truth across multiple frequency bands. The results are presented for low frequencies (Mel-SNR-L), mid frequencies (Mel-SNR-M), high frequencies (Mel-SNR-H), and an average of these three ranges is provided as the overall Mel-SNR-A.

5 Results

The performance metrics of the model, both in the frequency and time domains, with and without the implementation of the time-balanced loss, are summarized in Table 1. The model that operates in the time domain and incorporates the time-balanced loss exhibits superior performance. Consequently, only the outcomes from this particular configuration are reported for the other datasets.

As observed from Table 1 and Table 2, RFWave consistently outperforms in terms of PESQ scores, while Vocos routinely excels in UTMOS scores across different datasets. This might be due to the subtle biases inherent in these metrics. Additionally, it is observed that Vocos achieves superior performance in terms of Mel-SNR-M and Mel-SNR-H metrics, even when compared with RFWave₍₁₀₀₎ on the LibriTTS dataset, which utilizes 100 sampling steps. Nonetheless, upon examining the spectrograms in Figure 2, it is evident that RFWave produces more distinct harmonics at medium and high frequencies. The objective metrics pertaining to the samples can be found in Table A.1. This observation might be due to the fact that the Mel-SNR metric primarily assesses the accuracy of energy distribution across different frequencies without taking into account the precision of the phase information. Simultaneously, models such as Vocos perform better in spectral distance metrics due to their specific training aimed at content reconstruction. Conversely, diffusion-based methods, which do not employ feature or spectrogram matching, tend to generate samples that are more representative of the distribution, leading to more natural sounding audio [15].

We have trained the RFWave model on the Universal dataset employing 100-dimensional Mel spectrograms, as detailed in Section 4. Concurrently, we have also trained the model with 80-dimensional Mel spectrograms, which were extracted using the Espnet toolkit, a prevalent setup in Text-to-Speech (TTS) tasks. As evidenced in Table 2, the configuration of Mel spectrograms is impactful, with the 100-dimensional configuration demonstrating superior performance to the 80-dimensional one. Furthermore, the model yields satisfactory reconstructions for the Jamendo dataset. Online demos are available for further review³.

We performed inference speed benchmark tests using an Nvidia GeForce RTX 4090 GPU and an Intel Core i7-12700 CPU. The implementation was done in Pytorch [32], and no specific hardware optimizations were applied. The inference was carried out with a batch size of 1 sample, utilizing the LJSpeech test set. Table 1 displays the synthesis speed and model size of RFWave and Vocos. Vocos stands as a strong baseline given that it requires only a single forward pass and operates at the frame level.

Table 1: Objective metrics comparing the model’s performance in frequency and time domains with and without the time-balanced loss (frequency noted as freq, time-balanced loss noted as tbl).

Setting	UTMOS(↑)	PESQ(↑)	Mel-SNR-L(↑)	Mel-SNR-M(↑)	Mel-SNR-H(↑)	Mel-SNR-A(↑)
freq w/o tbl	3.61	3.60	15.43	16.94	18.09	16.80
freq w/ tbl	3.59	3.64	15.72	17.05	18.19	16.97
time w/o tbl	3.84	3.96	16.32	17.40	19.10	17.60
time w/ tbl	3.86	4.00	17.40	17.73	19.63	18.24
Vocos _(ISTFT)	4.09	3.54	16.71	18.44	20.64	18.57
groundtruth	4.39	-	-	-	-	-

³<https://bfs18.github.io/rfwave/>

Table 2: Objective evaluation metrics for RFWave and Vocos across various datasets. RFWave_(Espnet) utilizes the 80-dimension mel from Espnet as a conditional input. Meanwhile, RFWave₍₁₀₀₎ conducts sampling for 100 steps.

Dataset	Model	UTMOS(↑)	PESQ(↑)	Mel-SNR-L(↑)	Mel-SNR-M(↑)	Mel-SNR-H(↑)	Mel-SNR-A(↑)
Opencpop	RFWave	-	3.30	17.69	16.42	20.54	18.19
	Vocos _(ISTFT)	-	3.01	16.90	17.40	20.45	18.22
LibriTTS	RFWave	3.41	3.67	17.06	16.43	17.96	17.14
	RFWave ₍₁₀₀₎	3.51	3.98	19.17	17.97	20.86	19.29
	Vocos	3.74	3.31	17.20	18.81	20.87	18.81
Universal	RFWave	3.87	3.80	18.45	17.88	19.90	18.73
	RFWave _(Espnet)	3.75	3.40	16.43	16.54	17.20	16.71
Jamendo	RFWave	-	-	11.82	12.55	17.25	13.83

Table 3: Model footprint and synthesis speed. xRT stands for the speed at which the model can generate speech in comparison to real-time. A higher xRT value signifies that the model is capable of producing speech quicker than real-time, with a value of 1.0 representing the speed of real-time.

Model	parameters	GPU xRT(↑)	CPU xRT(↑)
RFWave	18.1 M	91.46	1.40
Vocos _(ISTFT)	13.5 M	2078.20	143.84

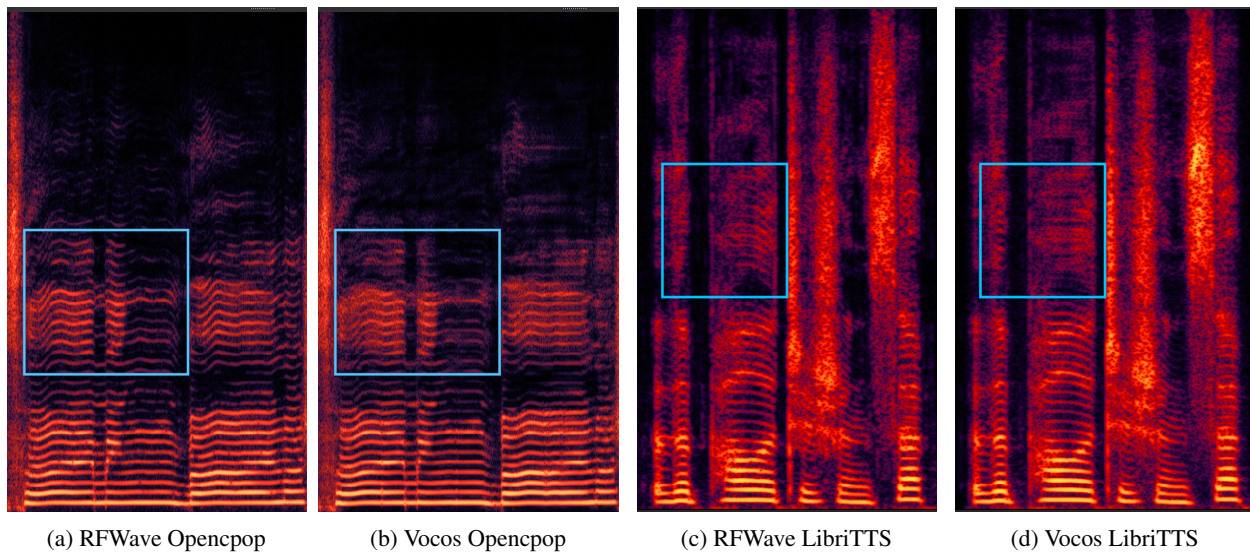


Figure 2: Examples of spectrograms. The differences are emphasized by blue rectangles. RFWave, in particular, produces clearer harmonics than Vocos, especially in the higher frequency range.

6 Conclusion and Discussion on Text-to-Speech

In this study, we propose RFWave, a multi-band Rectified Flow approach for audio waveform reconstruction. The model has been carefully designed to overcome the latency issues associated with diffusion models. RFWave stands out for its ability to generate complex spectrograms by operating at the frame level, processing all subbands concurrently. This concurrent processing significantly enhances the efficiency of the waveform reconstruction process. The empirical evaluations conducted in this research have demonstrated that RFWave achieves exceptional reconstruction quality. Moreover, it has shown superior computational efficiency by generating audio at a speed that is 90 times faster than real-time.

It would be relatively easy to implement the widely-used cascade pipeline to develop a text-to-speech (TTS) system. This involves mapping text features to Mel-spectrograms and then Mel-spectrograms to complex spectrograms using

Rectified Flow for both stages. Nevertheless, it is more advantageous to map text features directly to complex spectrograms, especially in the context of rapidly evolving large-scale TTS models. Large-scale TTS models typically incorporate extensive corpora, and eliminating one stage of processing can significantly reduce computational resource requirements. Additionally, this direct approach limits the discrepancies that can arise between the two stages. The infilling capabilities of Rectified Flow equip it to handle diverse functions similar to those managed by prominent large-scale TTS models, for example, replicating the speaker’s voice and speech style from a provided audio prompt. We have conducted preliminary experiments in developing a TTS system that maps text features directly to complex spectrograms based on Rectified Flow. Currently, the results do not match those of the cascade model. The code and model checkpoints are available in the repository. We believe this approach warrants further investigation and plan to explore it in future work.

References

- [1] Dario Rethage, Jordi Pons, and Xavier Serra. A wavenet for speech denoising. In *2018 IEEE International Conference on Acoustics, Speech and Signal Processing (ICASSP)*, pages 5069–5073. IEEE, 2018.
- [2] Masanori Morise, Fumiya Yokomori, and Kenji Ozawa. World: a vocoder-based high-quality speech synthesis system for real-time applications. *IEICE TRANSACTIONS on Information and Systems*, 99(7):1877–1884, 2016.
- [3] Nal Kalchbrenner, Erich Elsen, Karen Simonyan, Seb Noury, Norman Casagrande, Edward Lockhart, Florian Stimberg, Aaron Oord, Sander Dieleman, and Koray Kavukcuoglu. Efficient neural audio synthesis. In *International Conference on Machine Learning*, pages 2410–2419. PMLR, 2018.
- [4] Aaron Oord, Yazhe Li, Igor Babuschkin, Karen Simonyan, Oriol Vinyals, Koray Kavukcuoglu, George Driessche, Edward Lockhart, Luis Cobo, Florian Stimberg, et al. Parallel wavenet: Fast high-fidelity speech synthesis. In *International conference on machine learning*, pages 3918–3926. PMLR, 2018.
- [5] Wei Ping, Kainan Peng, and Jitong Chen. Clarinet: Parallel wave generation in end-to-end text-to-speech. *arXiv preprint arXiv:1807.07281*, 2018.
- [6] Ian Goodfellow, Jean Pouget-Abadie, Mehdi Mirza, Bing Xu, David Warde-Farley, Sherjil Ozair, Aaron Courville, and Yoshua Bengio. Generative adversarial nets. In Z. Ghahramani, M. Welling, C. Cortes, N. Lawrence, and K.Q. Weinberger, editors, *Advances in Neural Information Processing Systems*, volume 27. Curran Associates, Inc., 2014.
- [7] Kundan Kumar, Rithesh Kumar, Thibault De Boissiere, Lucas Gestin, Wei Zhen Teoh, Jose Sotelo, Alexandre De Brebisson, Yoshua Bengio, and Aaron C Courville. Melgan: Generative adversarial networks for conditional waveform synthesis. *Advances in neural information processing systems*, 32, 2019.
- [8] Ryuichi Yamamoto, Eunwoo Song, and Jae-Min Kim. Parallel wavegan: A fast waveform generation model based on generative adversarial networks with multi-resolution spectrogram. In *ICASSP 2020-2020 IEEE International Conference on Acoustics, Speech and Signal Processing (ICASSP)*, pages 6199–6203. IEEE, 2020.
- [9] Jungil Kong, Jaehyeon Kim, and Jaekyoung Bae. Hifi-gan: Generative adversarial networks for efficient and high fidelity speech synthesis. *Advances in Neural Information Processing Systems*, 33:17022–17033, 2020.
- [10] Takuhiro Kaneko, Kou Tanaka, Hirokazu Kameoka, and Shogo Seki. istftnet: Fast and lightweight mel-spectrogram vocoder incorporating inverse short-time fourier transform. In *ICASSP 2022-2022 IEEE International Conference on Acoustics, Speech and Signal Processing (ICASSP)*, pages 6207–6211. IEEE, 2022.
- [11] Hubert Siuzdak. Vocos: Closing the gap between time-domain and fourier-based neural vocoders for high-quality audio synthesis. *CoRR*, abs/2306.00814, 2023.
- [12] Hui-Peng Du, Ye-Xin Lu, Yang Ai, and Zhen-Hua Ling. Apnet2: High-quality and high-efficiency neural vocoder with direct prediction of amplitude and phase spectra. *arXiv preprint arXiv:2311.11545*, 2023.
- [13] Zhifeng Kong, Wei Ping, Jiaji Huang, Kexin Zhao, and Bryan Catanzaro. Diffwave: A versatile diffusion model for audio synthesis. *arXiv preprint arXiv:2009.09761*, 2020.
- [14] Nanxin Chen, Yu Zhang, Heiga Zen, Ron J Weiss, Mohammad Norouzi, and William Chan. Wavegrad: Estimating gradients for waveform generation. *arXiv preprint arXiv:2009.00713*, 2020.
- [15] Robin San Roman, Yossi Adi, Antoine Deleforge, Romain Serizel, Gabriel Synnaeve, and Alexandre Défossez. From discrete tokens to high-fidelity audio using multi-band diffusion. In *Thirty-seventh Conference on Neural Information Processing Systems*, 2023.
- [16] Xingchao Liu, Chengyue Gong, and Qiang Liu. Flow straight and fast: Learning to generate and transfer data with rectified flow. In *The Eleventh International Conference on Learning Representations, ICLR 2023, Kigali, Rwanda, May 1-5, 2023*. OpenReview.net, 2023.
- [17] Geng Yang, Shan Yang, Kai Liu, Peng Fang, Wei Chen, and Lei Xie. Multi-band melgan: Faster waveform generation for high-quality text-to-speech. In *2021 IEEE Spoken Language Technology Workshop (SLT)*, pages 492–498, 2021.
- [18] J. Johnston. A filter family designed for use in quadrature mirror filter banks. In *ICASSP '80. IEEE International Conference on Acoustics, Speech, and Signal Processing*, volume 5, pages 291–294, 1980.
- [19] Sanghyun Woo, Shoubhik Debnath, Ronghang Hu, Xinlei Chen, Zhuang Liu, In So Kweon, and Saining Xie. Convnext V2: co-designing and scaling convnets with masked autoencoders. In *IEEE/CVF Conference on Computer Vision and Pattern Recognition, CVPR 2023, Vancouver, BC, Canada, June 17-24, 2023*, pages 16133–16142. IEEE, 2023.

- [20] Alexandre Défossez, Jade Copet, Gabriel Synnaeve, and Yossi Adi. High fidelity neural audio compression. *CoRR*, abs/2210.13438, 2022.
- [21] Diederik Kingma, Tim Salimans, Ben Poole, and Jonathan Ho. Variational diffusion models. In M. Ranzato, A. Beygelzimer, Y. Dauphin, P.S. Liang, and J. Wortman Vaughan, editors, *Advances in Neural Information Processing Systems*, volume 34, pages 21696–21707. Curran Associates, Inc., 2021.
- [22] Jingjing Xu, Xu Sun, Zhiyuan Zhang, Guangxiang Zhao, and Junyang Lin. Understanding and improving layer normalization. In H. Wallach, H. Larochelle, A. Beygelzimer, F. d'Alché-Buc, E. Fox, and R. Garnett, editors, *Advances in Neural Information Processing Systems*, volume 32. Curran Associates, Inc., 2019.
- [23] Keith Ito and Linda Johnson. The lj speech dataset. <https://keithito.com/LJ-Speech-Dataset/>, 2017.
- [24] Yu Wang, Xinsheng Wang, Pengcheng Zhu, Jie Wu, Hanzhao Li, Heyang Xue, Yongmao Zhang, Lei Xie, and Mengxiao Bi. Opencpop: A high-quality open source chinese popular song corpus for singing voice synthesis. In Hanseok Ko and John H. L. Hansen, editors, *Interspeech 2022, 23rd Annual Conference of the International Speech Communication Association, Incheon, Korea, 18-22 September 2022*, pages 4242–4246. ISCA, 2022.
- [25] Dmitry Bogdanov, Minz Won, Philip Tovstogan, Alastair Porter, and Xavier Serra. The mtg-jamendo dataset for automatic music tagging. In *Machine Learning for Music Discovery Workshop, International Conference on Machine Learning (ICML 2019)*, Long Beach, CA, United States, 2019.
- [26] Yuma Koizumi, Heiga Zen, Shigeki Karita, Yifan Ding, Kohei Yatabe, Nobuyuki Morioka, Michiel Bacchiani, Yu Zhang, Wei Han, and Ankur Bapna. Libritts-r: A restored multi-speaker text-to-speech corpus. *arXiv preprint arXiv:2305.18802*, 2023.
- [27] Yao Shi, Hui Bu, Xin Xu, Shaoji Zhang, and Ming Li. Aishell-3: A multi-speaker mandarin tts corpus and the baselines. *arXiv preprint arXiv:2010.11567*, 2020.
- [28] Junichi Yamagishi, Christophe Veaux, and Kirsten MacDonald. Cstr vctk corpus: English multi-speaker corpus for cstr voice cloning toolkit (version 0.92). 2019.
- [29] Haohe Liu, Qiuqiang Kong, Qiao Tian, Yan Zhao, DeLiang Wang, Chuanzeng Huang, and Yuxuan Wang. Voicefixer: Toward general speech restoration with neural vocoder. *arXiv preprint arXiv:2109.13731*, 2021.
- [30] Chanwoo Kim and Richard M Stern. Robust signal-to-noise ratio estimation based on waveform amplitude distribution analysis. In *Ninth Annual Conference of the International Speech Communication Association*. Citeseer, 2008.
- [31] Takaaki Saeki, Detai Xin, Wataru Nakata, Tomoki Koriyama, Shinnosuke Takamichi, and Hiroshi Saruwatari. UTMOS: utokyo-sarulab system for voicemos challenge 2022. In Hanseok Ko and John H. L. Hansen, editors, *Interspeech 2022, 23rd Annual Conference of the International Speech Communication Association, Incheon, Korea, 18-22 September 2022*, pages 4521–4525. ISCA, 2022.
- [32] Ian Goodfellow, Jean Pouget-Abadie, Mehdi Mirza, Bing Xu, David Warde-Farley, Sherjil Ozair, Aaron Courville, and Yoshua Bengio. Generative adversarial nets. In Z. Ghahramani, M. Welling, C. Cortes, N. Lawrence, and K.Q. Weinberger, editors, *Advances in Neural Information Processing Systems*, volume 27. Curran Associates, Inc., 2014.

A Supplementary Material

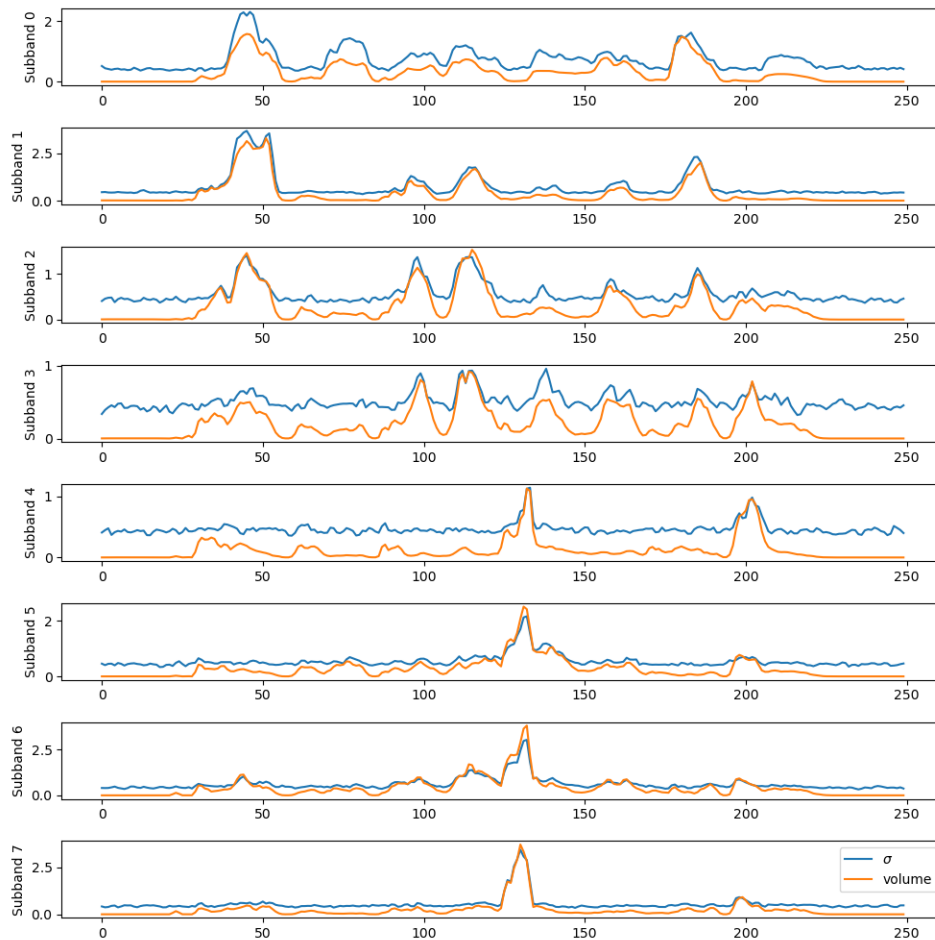


Figure A.1: The Volume and σ exhibit consistent variation across the frames.

Table A.1: Objective metrics for the two sentences as evaluated across different models.

Data	Model	UTMOS(\uparrow)	PESQ(\uparrow)	Mel-SNR-L(\uparrow)	Mel-SNR-M(\uparrow)	Mel-SNR-H(\uparrow)	Mel-SNR-A(\uparrow)
Opencpop 2009000326	RFWave	-	3.54	18.31	16.44	20.14	18.27
	Vocos _(ISTFT)	-	3.25	17.40	17.16	19.39	17.96
LibriTTS 121_121726_000005_000001	RFWave	3.87	3.71	17.73	16.97	17.97	17.55
	Vocos _(ISTFT)	4.23	3.75	19.76	19.72	20.32	19.94